Optimizing landslide susceptibility zonation: Effects of DEM spatial resolution and slope unit delineation on logistic...

Article *in* Geomorphology · October 2017

DOI: 10.1016/j.geomorph.2017.10.018

6 authors, including:

Ivan Marchesini
Italian National Research Council
98 PUBLICATIONS **362** CITATIONS
SEE PROFILE

M. Alvioli
Italian National Research Council
70 PUBLICATIONS **545** CITATIONS
SEE PROFILE

Mauro Rossi
Italian National Research Council
149 PUBLICATIONS **3,085** CITATIONS
SEE PROFILE

J.-P. Malet
CNRS / University of Strasbourg
385 PUBLICATIONS **3,547** CITATIONS
SEE PROFILE

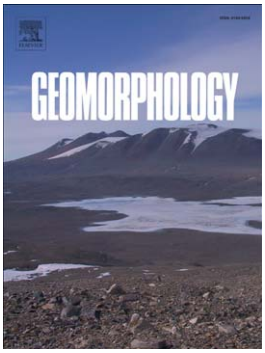

Optimizing landslide susceptibility zonation: Effects of DEM spatial resolution and slope unit delineation on logistic regression models

R. Schlögel, I. Marchesini, M. Alvioli, P. Reichenbach, M. Rossi, J.-P. Malet

PII: S0169-555X(16)30665-1
DOI: doi:10.1016/j.geomorph.2017.10.018
Reference: GEOMOR 6204

To appear in: *Geomorphology*

Received date: 29 July 2016
Revised date: 10 July 2017
Accepted date: 24 October 2017

Please cite this article as: Schlögel, R., Marchesini, I., Alvioli, M., Reichenbach, P., Rossi, M., Malet, J.-P., Optimizing landslide susceptibility zonation: Effects of DEM spatial resolution and slope unit delineation on logistic regression models, *Geomorphology* (2017), doi:10.1016/j.geomorph.2017.10.018

Optimizing landslide susceptibility zonation: effects of DEM spatial resolution and slope unit delineation on logistic regression models

Schlögel, R.[1,2,*], Marchesini, I.[3], Alvioli, M.[3], Reichenbach, P.[3], Rossi, M.[3], Malet, J.-P.[2]

[1] EURAC Research, Institute for Earth Observation, Viale Druso 1, 39100 Bolzano, Italy

[2] Institut de Physique du Globe de Strasbourg, UMR7516, Université de Strasbourg/EOST, CNRS, 5 rue René Descartes, 67084 Strasbourg, Cedex, France

[3] Consiglio Nazionale delle Ricerche, Istituto di Ricerca per la Protezione Idrogeologica, via Madonna Alta 126, 06128 Perugia, Italy

[*] romy.schlogel@gmail.com

Abstract

We perform landslide susceptibility zonation with slope units using three digital elevation models (DEMs) of varying spatial resolution of the Ubaye Valley (South French Alps). In so doing, we applied a recently developed algorithm automating slope unit delineation, given a number of parameters, in order to optimize simultaneously the partitioning of the terrain and the performance of a logistic regression susceptibility model. The method allowed us to obtain optimal slope units for each available DEM spatial resolution. For each resolution, we studied the susceptibility model performance by

analyzing in detail the relevance of the conditioning variables. The analysis is based on landslide morphology data, considering either the whole landslide or only the source area outline as inputs. The procedure allowed us to select the most useful information, in terms of DEM spatial resolution, thematic variables and landslide inventory, in order to obtain the most reliable slope unit-based landslide susceptibility assessment.

Keywords:

Landslide susceptibility; DEM spatial resolution; Statistical significance; Slope units; Ubaye valley

1. Introduction

Landslide susceptibility represents the likelihood of landslide occurrence in an area, evaluated on the basis of local terrain conditions (e.g., relief, hydrology, lithology, and land use) and known landslide locations. According to Fell et al. (2008), susceptibility zonation involves the spatial distribution and rating of the terrain units according to their propensity to produce landslides. Statistical susceptibility models usually perform best for large areas and where the relationships between determining factors and landslide occurrence are complex (Guzzetti et al., 1999). The preparation of susceptibility maps requires a number of choices regarding: (i) landslide conditioning factors, including local topography, represented by a Digital Elevation Model (DEM); (ii) type and size of mapping units; (iii) a statistical model to classify the mapping units and (iv) characteristics of the landslide inventory.

The conditioning factors, defined as the terrain properties that evolve to bring the slope to a marginally stable state (Fell et al., 2008), are important variables for landslide susceptibility zonation. The main categories of these predictor variables are geology, land use and topography expressed in terms of slope gradient, slope aspect and slope curvature (Claessens et al., 2005; Fuchs et al., 2014). These last

variables are derived from a morphometric analysis of both relief and landslides, the cartographic representation of which becomes less accurate when the pixel size increases (Legorreta Paulìn et al., 2010). The selection of a proper DEM is important in many susceptibility zonations. Dietrich et al. (2001) compared the location of shallow landslides using different DEM spatial resolutions (i.e. 30 versus 6 m and 10 versus 2 m). They found that classification results were similar for the moderate landslide susceptibility class for both coarse and fine DEM resolutions; however, with the finer DEM spatial resolution, the classification results were strongly dependent on the local ridges and valleys topography. Claessens et al. (2005) analyzed the effects of DEM spatial resolution on the results of a model that simulates spatially explicit shallow landslide hazard and soil redistribution quantities. They analyzed the slope distribution, specific catchment area and relative hazard for four different DEM resolutions. When the extents of the slopes with low and high hazards are compared, finer DEM resolutions and higher landslide hazard thresholds have the effect of increasing the extent of the areas considered as stable. This artifact is due to a higher number of cells and thus to a lower probability for a grid cell within a given territory to be affected by a landslide. Consequently, the identification of a meaningful DEM spatial resolution is often not possible because no spatial resolution can, even for small areas of interest, represent the size of all possible landslides. According to Tian et al. (2008), a finer resolution does not necessarily lead to a higher accuracy in terms of landslide susceptibility. Studying DEM resolutions ranging from 5 to 190 m, they found that the classification accuracy shows a W-shaped curve as a function of DEM resolution. While the accuracy decreases as the DEM resolution increases from 5 to 70 m, it reaches its optimum value for a 90 m DEM corresponding to the mean size of the landslides. Catani et al. (2013) found the best compromise between landslide size and landslide conditioning variables using a range of spatial resolutions from 50 to 100 m (i.e. with area under the curve (*AUC*) of the receiver operating characteristic values of 0.88 and 0.81, respectively) in

comparison to finer resolutions from 10 to 20 m (i.e. *AUC* = 0.54 and 0.58). The current availability of freely accessible DEMs also poses the question of their accuracy for landslide susceptibility analyses.

The selection of meaningful mapping units is of great importance for susceptibility zonation. Mapping units should maximize the within-unit (internal) homogeneity and the between-unit (external) heterogeneity across the area of interest (Guzzetti et al., 1999; Guzzetti, 2006). In the literature, authors have proposed single pixel (Ercanoglu, 2005), groups of neighboring pixels, or polygons with common characteristics as mapping units (van den Eeckhaut et al., 2009). Extensive reviews discussing this subject are provided by Guzzetti et al. (1999), Aleotti and Chowdhury (1999) and Brenning (2005).

Each different category of mapping units (pixel- or polygon-based) present advantages and disadvantages. In the pixel-based approaches, grids usually do not represent a physical property of the terrain; the grid size is dictated by the available DEM spatial resolution. Moreover, the current trend of using small grid cells is unjustified most of the time; the appropriate mapping unit size and spatial resolution for the analysis should be determined considering the range of landslide sizes, the targeted scale of the susceptibility map and the mapping accuracy of the conditioning factors (Tian et al., 2008). In a polygon-based approach, slope units (SUs) are defined according to the hydrological and geomorphological conditions of the area of interest (Carrara et al., 1991; Carrara et al., 1995; Guzzetti et al., 1999; Guzzetti, 2006) and are thus bounded by the main drainage and divide lines. SUs are particularly useful when the available DEM is recent with respect to the date of the landslide inventory. In that case the use of pixel-based approaches has the effect of introducing topography variables in the classifier, including the signature of landslides. As a consequence, the resulting statistical model may be able to detect possible landslide bodies or source areas but not to predict where future independent

landslides may occur. As the SU-based approach considers the totality of the slopes where the landslides occurred, it is much less affected by this type of bias.

Several data-driven statistical models have been proposed in the literature for landslide susceptibility evaluation (Aleotti and Chowdhury 1999; Guzzetti et al., 1999; Kanungo et al. 2009). They include logistic or multiple regression, discriminant analysis, conditional analysis, decision trees, artificial neural networks and support vector machine approaches (Pardeshi et al., 2013). Brenning (2005) reviewed the literature on statistical models and concluded that logistic regression and discriminant analysis were the most frequently used classifiers. The quality of the model has to be quantified using validation procedures in order to estimate its reliability, robustness, degree of fitting and prediction skills. The most commonly used cutoff-independent performance criteria used for evaluating model performance are the receiver operating characteristic curves and the success-rate curves (Frattini et al., 2010; Corominas et al., 2014). According to Legorreta Paulín et al. (2016), *AUC* better measures predictive capability for logistic regression models; here we used *AUC* as a metric to assess the overall quality of a model (Hanley and McNeil, 1982).

Selection of conditioning factors, mapping units and a statistical model constitutes an operational method (Corominas et al., 2014). In this work, we propose an operational procedure to evaluate the effects of DEM spatial resolution, significance of conditioning variables and of information from a landslide inventory. SU delineation and optimization of the shapes and sizes of SUs were performed with existing software, for each DEM resolution and grouping variable in the statistical model. We suggest that our procedure can be used to optimize the preparation of a landslide susceptibility zonation, taking the maximum advantage of available information in the conditioning factors and in the landslide inventory.

The procedure was tested on a study area located in the middle part of the Ubaye Valley (South French Alps). Our analysis was based on the following pre-conditions: (i) availability of a complete geomorphological landslide inventory for the period 1950–2012 in which both the landslide source areas and the landslide bodies are recorded (Schlögel et al., 2015); (ii) division of the terrain into SUs, since the aim is to classify the terrain into regions with different susceptibility at the moderate scale of 1:10.000 to be compliant with the French regulations of hazard and risk mapping (Malet et al., 2006); and (iii) use of a data-driven statistical model for the susceptibility zonation. The procedure is applied to three DEMs of different spatial resolutions and quality, obtained from different sources.

2. Study area and data

2.1. Physio-geographic settings of the study area

The study area (ca. 257.6 km^2) is situated in the middle part of the Ubaye Valley (Fig. 1a), an intra-Alpine mountainous zone of the French Alps. The area is characterized by highly variable rainfall amounts (from 400 to 1300 mm yr^{-1}), with intense storms in summer and autumn. Typical elevations range from 2200 to 2600 m with the highest peaks reaching almost 2900 m. The area constitutes a geological window, baring the autochthonous Callovo-Oxfordian black marls (Terres Noires), under the allochthonous formation of the Autapie and Parpaillon sandstones (Maquaire et al., 2003). Fig. 1b shows a simplified lithological map where rock and soil formations are classified in six classes: torrential and lacustrine deposits, blocks and screes, weathered marls, moraine deposits, limestone and marly-limestone, gypsum, sandstone and some rare outcrops of quartzite.

The slopes, affected by different landslide types (Flageollet et al., 1999; Fig. 1a), can be subdivided in two morphological sections:

(a) Lower parts (1100–1900 m a.s.l.; see upper contour line limit in Fig. 1a): slopes are gentle (10–30°) and consist of black marls (Fig. 1b) with fragile plates and flakes in a clayed matrix. Slopes are mostly covered by thick Quaternary talus deposits originated from poorly sorted moraine deposits (Fig. 1b) with some landslide debris. Due to the high erosion rate of marls, badlands are observed.

(b) In the upper parts (1900–3000 m a.s.l.), slopes are steeper than 45° and consist of thrust sheets of cataclastic calcareous sandstones (Fig. 1b), often covered by unconsolidated debris (blocks or screes) with thickness ranging from 0.5 to 5 m. Outcrops of limestones are barely observed at lower elevations.

Around 40% of the area is covered by forests; grasslands and arable lands are present for about 25% and 5%, respectively. The remaining types (30%) are bare soils and urbanized areas. We have classified the land use into five types (Fig. 1c): forest, arable land, grassland, bare rock and 'other', such as built up areas and water features.

2.2. Landslide inventory map

The geological, structural and climatological settings in the study area are favorable for landslides (Flageollet et al., 1999) and torrential activity (Remaître et al., 2005; Remaître and Malet, 2010). In this work, we consider the landslides mapped by Thiery et al. (2007) for years before 2004 and later updated with 2004-2009 data (Schlögel et al., 2015). Multisource data were used for creating an overall landslide inventory including archives (reports and local measurements), field mapping, visual interpretation of aerial ortho-photographs and images from aerial radar elevation data, and SAR interferometry deformation maps. The inventory was prepared mainly by visual analysis of the 2004

and 2009 aerial ortho-photographs to detect new and remobilized failures. In the inventory map, only the landslides considered as active or formed during the past 50 years were included. In total, 662 active rotational and translational landslides were mapped; these have a mean area of 32,000 m² and cover a region of around 21 km²; 8.2% of the region corresponds to landslide bodies. The source areas (density of 1.7%) were then mapped based on the depletion zones visible on the aerial ortho-photographs, elevation data and fieldwork. These source areas occupy 20.5% of the total landslide areas.

2.3. DEMs

Various DEMs are available for the territory of interest and were used to characterize the relief at different spatial scales. The DEMs were acquired using distinct methodologies and technologies. We used DEMs of three spatial resolutions: a 5 m airborne DEM (IfSAR[1]), a 10-m DEM (IfSAR and 5-m DSM contour interpolation) and a 25-m DEM from BDAlti® IGN[2], the French Mapping Agency.

- The 5-m DEM was acquired from an Interferometric Synthetic Aperture Radar (IfSAR) survey carried out in 2008 using airborne radar antennas. The IfSAR Type II (InterMap, 2008) provides a 5 m spatial resolution with a vertical root mean square error value of 1 m. Processing steps completed by the data provider corrected the original data using the denoising algorithm of Stevenson et al. (2010) to avoid artifacts due to radar data acquisition (Maire et al., 2003). Vegetation, buildings and man-made features were removed from the raw data using filtering algorithms to maintain original areas. The final DEM is available in the Lambert NTF zone III projection which is a Lambert Conformal Conic projection used in South France and based on the Clarke 1880 ellipsoid.

1 http://gis.icao.int/icaoetod/INTERMAP_IFSAR_Data_Collection_English.pdf
2 http://professionnels.ign.fr/bdalti

- The 10-m DEM was constructed as follows. Thiery (2007) prepared a hybrid digital terrain model at 10-m resolution from multiple sources including contour lines digitized from local topographic maps at 1:25,000 scale (Scan25, IGN). The topographic maps were created from a stereo-photogrammetric construction of the relief from high resolution aerial optical photographs (1:20,000 to 1:60,000; BDAlti® v.1 metadata). A representation of the topographic maps at a 1:10,000 scale is available from IGN and delivered on A0 sheets. The sheets were scanned and georeferenced using at least 20 ground control points per sheet. The horizontal accuracy of the georeferencing is 1 m. The 10-m spacing elevation lines were then digitized. Intermediate contour lines were manually added to guide the interpolation in flat areas (Ubaye river) or in thalwegs of torrents in order to obtain the best representation of the topographic surface (Thiery, 2007). The polylines were then transformed in triplets (X,Y,Z) of elevation points with a spacing of 2 m along the length of the lines. For some local spots not covered by the topographic maps, the elevation points of the IfSAR DEM were integrated in the point cloud database. The two sets of elevation points (digitized elevation lines, IfSAR) were then combined using the Iterative Closest Point alignment algorithm (e.g. Polyworks[3]). The aligned point cloud was then interpolated with ordinary kriging and a semi-variogram (Krige, 1966; Baillargeon, 2005) that provided the best results in terms of accuracy (Thiery, 2007). The final DEM was projected in the Lambert NTF zone III coordinate reference system.
- The 25-m DEM is the free open source elevation reference model of the French territory created by stereo photogrammetry applied to high resolution airborne optical photographs (1:20,000 to 1:60,000; BDAlti® v.1 metadata). The elevation information was generalized by IGN to produce a 25-m grid DEM. The estimated vertical accuracy of the DEM is 4.0 to 5.2 m in mountainous areas. The DEM is available in Lambert-93 coordinate system which is a Lambert

[3] http://www.innovmetric.com/

Conformal Conic projection using the RGF93 geoid (IAG GRS 1980 ellipsoid, based on Greenwich meridian). The projection to Lambert NTF zone III was performed with Global Mapper[4]; the 25-m grid resolution was preserved by using a bilinear geographic transformation.

3. Partitioning of the terrain in slope units

SUs can be defined by manual procedures (which are intrinsically error-prone and subjective) or by using specialized terrain analysis software. We used the *r.slopeunits* software module for SU delineation developed by Alvioli et al. (2016) to be used in the GRASS GIS (GRASS Development Team, 2016) environment. The method defines SUs bounded by hydrological drainage and divide lines, maximizing the intra-unit (internal) homogeneity and the inter-unit (external) heterogeneity of the slope aspect.

For a given landscape, no unique SU delineation exists as it depends on the purpose of the study and the scale at which the study is carried over. For this reason, the *r.slopeunits* software adopts an iterative and adaptive algorithm for which the user can define: (i) the required degree of homogeneity within each SU with the parameter *c* representing the minimum circular variance of the slope aspect, and (ii) the tentative minimum size of the SU (*a*, in m^2). The iterative analysis starts by checking half-basins defined by a large flow accumulation threshold against user-defined homogeneity and size requirements; the threshold is then decreased for those half-basins that did not meet user requirements and the conditions are checked again at the next iteration. The process is repeated until the whole study area is partitioned into SUs, i.e. half-basins meeting user requirements. The algorithm is also adaptive, since the user requirements are met for different values of the flow accumulation threshold in different regions of the study area, depending on local terrain conditions, producing SUs with varying size in

[4] http://www.globalmapper.com

different regions of the study area. Other parameters such as the flow accumulation threshold, a reduction factor tuning the rate of decrease of the accumulation threshold in the iterative algorithm, and a minimum size below which SUs are merged with the neighboring ones at the end of the iterations are required by the *r.slopeunits* software; these are not described here as we focus on the determination of the best combination of the *c* and *a* parameter values, directly related to the terrain morphology, following the approach of Alvioli et al. (2016). Technical details of the algorithm are described in Alvioli et al. (2016). The values of (*a*, *c*) parameters are determined by maximization of a proper objective function, providing the optimal SU delineation for the given DEM, thematic variables, landslide inventory and landslide susceptibility model.

4. Landslide susceptibility modeling

The objective of our landslide susceptibility assessment is to propose a ranking of the SUs in terms of their propensity to landslide initiation that can be used for regulatory prevention maps at the scale of 1:10,000 (e.g. Plan de Prévention des Risques / PPR; Malet et al., 2006). In this context, we decided to quantify landslide susceptibility with the Logistic Regression Model (LRM) implemented by Rossi et al. (2010) (available at [5]) and used in Alvioli et al. (2016) (available at [6]), and to create SUs of minimum and maximum sizes of, respectively, 10,000 and 550,000 m^2.

LRMs have been applied for susceptibility mapping by various researchers, including for instance Cox (1958); Bernknopf et al. (1988); Wieczorek et al. (1996); Guzzetti et al. (1999); Ohlmacher and Davis (2003); Ayalew and Yamagishi (2005); Rossi et al. (2010); Rossi and Reichenbach (2016). LRMs investigate relationships among dependent (landslide presence/absence) and independent landslide conditioning factors. We performed the analysis by formulating two different ways of using the

[5] http://geomorphology.irpi.cnr.it/tools/landslide-susceptibility-assessment
[6] http://geomorphology.irpi.cnr.it/tools/slope-units

landslide inventory data to select unstable SUs: (i) using whole landslide body information, in which case an SU is considered unstable if more than 8.5% of its surface area is covered by landslides, and stable otherwise; (ii) using the landslide sole source area, in which case an SU is considered unstable if more than 0.01% of its area is covered by landslide source areas, effectively using the presence/absence of source areas as a criterion for instability/stability. Each SU was characterized by statistics calculated for all the conditioning variables. The slope gradients and the planar (or longitudinal) and profile (or cross) curvatures were calculated for each grid cell of the three DEMs.

5. Effect of DEM resolution and terrain partitioning on landslide susceptibility zonation

To analyze the influence of DEM spatial resolution and of the SU partitioning on landslide susceptibility, we calculated susceptibility maps with an optimal SU delineation for each available DEM. The optimal SU delineation was obtained by analyzing several SU delineations, corresponding to several combinations of the input parameters of the *r.slopeunits* software, and choosing the best one by means of well-defined criteria. For the three DEMs, we ran the *r.slopeunits* with different values of c = (0.01, 0.05, 0.10, 0.15, 0.25, 0.35, 0.45) and a = (10,000 m^2, 50,000 m^2, 100,000 m^2, 150,000 m^2, 250,000 m^2, 350,000 m^2, 450,000 m^2, 550,000 m^2) for a total of 56 combinations, corresponding to 56 SU delineations, differing for SU number, shape and size. These values were determined heuristically, as all of them provide SU delineations that are morphologically plausible by visual interpretation, in addition to being hydrologically correct by construction.

Fig. 2 presents, for each DEM, 16 SU delineations for the selected (a, c) parameter combinations. The results illustrate that small values of c typically produce small SUs, and the same holds for small a.

Larger SUs are obtained with large values of *c* and *a*. This statement is quantified and illustrated in the box plots of Fig. 3.

The choice of the best combination of (*a, c*) parameters is not possible only with a visual analysis of the maps presented in Figs. 2 and 3. Therefore, following Alvioli et al. (2016), we used a procedure that simultaneously optimizes: (i) the homogeneity/inhomogeneity requirements for a proper SU delineation, and (ii) the performance of the susceptibility model (Alvioli et al., 2016). This procedure makes use of two metrics.

The performance of the *r.slopeunits* algorithm in segmenting the aspect map is measured by the metric *F*(*a, c*), introduced by Espindola et al. (2006) for the segmentation of digital images and adapted by Alvioli et al. (2016) to work with the aspect circular variance. The segmentation metric *F*(*a, c*) is obtained by means of the local aspect variance *V*, and the autocorrelation index *I*, defined as follows:

$$V = \frac{\sum_n c_n s_n}{\sum_n s_n} \tag{1}$$

and

$$I = \frac{N \sum_{n,l} \omega_{nl} (\alpha_n - \bar{\alpha})(\alpha_l - \bar{\alpha})}{(\sum_n (\alpha_n - \bar{\alpha})^2) \sum_{n,l} \omega_{nl}}, \tag{2}$$

where *n* labels all the *N* SUs in the given set; c_n, s_n and α_n are the circular variance of the aspect, the surface area and the average aspect of the *n*-th SU; $\bar{\alpha}$ is the average aspect of the whole study area; ω_{nl} is an indicator for spatial proximity, equal to unity if SU polygons *n* and *l* are adjacent, zero otherwise. Thefunctions *V* and *I* both depend on the (*a, c*) parameters, by construction; *V*(*a, c*) measures internal aspect variance and assigns more importance to large SUs, avoiding numerical instabilities produced by small ones, while *I* measures external aspect variance and has minima for SU sets exhibiting well-defined aspect boundaries between adjacent SUs. The overall aspect segmentation metric is defined as:

$$F(a,c) = \frac{V_{max} - V(a,c)}{V_{max} - V_{min}} + \frac{I_{max} - I(a,c)}{I_{max} - I_{min}}, \quad (3)$$

where the maximum and minimum of both *V* and *I* functions are relative to the (*a*, *c*) combinations considered in the analysis.

The performance of the susceptibility model for a given SU delineation is measured by the *AUC* of the receiver operating characteristic, with numerical value denoted by *R*(*a*, *c*), which is a standard metric for binary classifiers. The two metrics are calculated as a function of the (*c*, *a*) parameters and the combination $S(a,c) = F'(a,c)\,R'(a,c)$ is obtained, where the dash indicates original functions scaled by their maximum values, in order to make them comparable:

$$\begin{cases} F'(a,c) = F(a,c)/F_{max} \\ R'(a,c) = R(a,c)/R_{max} \end{cases}. \quad (4)$$

The objective function *S*(*a*, *c*) was maximized to define optimal (*a*, *c*) input parameters for each of the three DEM spatial resolutions. The function *R*(*a*, *c*) depends on the landslide inventory, thus it must be calculated separately for the two cases in which (i) the whole landslide bodies, or (ii) only the source area is taken into account, to distinguish stable/unstable SUs, while the function *F*(*a*, *c*) is common to the two cases.

6. Results and discussion

We investigated which DEM spatial resolution and SU partition are more suitable for landslide susceptibility zonation considering the available conditioning factors and landslide inventory, applying a logistic regression model. In particular, we systematically analyzed the effects of (i) three DEM spatial resolutions; (ii) the use of either landslide bodies or landslide source areas as the grouping (dependent) variable, i.e. the quantity used to flag each SU polygon as stable or unstable in the model calibration stage; and (iii) the relative significance of the different conditioning variables in each LRM.

We adopted the *r.slopeunits software*, and the optimization procedure of the input parameters, from Alvioli et al. (2016). The analysis as a function of the (*a*, *c*) parameters or *r.slopeunits* is only intended here as a technical step aimed at determining the optimal SU delineation for each (i) DEM resolution, and (ii) different grouping variable (i.e. landslide body or source area). The significance analysis of the conditioning variables used to apply the LRM was also conducted as a function of the (*a*,*c*) parameters. This is novel with respect to the method of Alvioli et al. (2016), and it was used to eventually select the best DEM resolution for our case study.

Figs. 4 and 5 present, for the three DEMS, the segmentation metric $F(a, c)$, *AUC* $R(a, c)$ and their combination $S(a, c)$ calculated for the selected values of *c* (in the range 0.01-0.45) and *a* (in the range 10,000-550,000 m^2). Figs. 4 and 5 show the results of the susceptibility models calculated using (respectively) either landslide bodies or landslide source areas as a grouping variable. The segmentation metric is presented only in Fig. 4 because it does not depend on the grouping variable. The analysis of the graphs allowed identifying optimal combinations of *c* and *a* that maximized $S(a, c)$ (Table 1).

Table 2 describes the average and the standard deviations of the SU sizes obtained for the optimal combination of parameters identified in Table 1. We observe that while the average size is positively and almost linearly correlated with the spatial resolution of the DEMs, the standard deviation is larger using the 10 m resolution DEM, irrespective of the grouping variable.

Figs. 4 and 5 show that the *AUC* metric computed within the susceptibility models exhibits similar values for all the 56 combinations of (*a*, *c*) parameters and for both the landslide bodies and source

areas grouping. The optimal combination of parameters a and c that maximize $S(a, c)$ reveals little variation for whether landslide bodies or source areas were used, and are different for the three DEMs.

Figs. 4 and 5 also indicate that there is a range of (a, c) parameter combinations where the $S(a, c)$ values are relatively very low, and not acceptable. In particular, values of circular variance greater than $c = 0.2$ result in unreliable SU delineation.

Investigation of the significance of different conditioning variables (p-value < 0.05) for each run of the LRM (Fig. 6) indicates that:

(i) the susceptibility results obtained using large SUs (high values of a and c) have a low percentage of significant conditioning factors, whereas the percentage of significant conditioning factors increases up to 40% for results obtained using small SUs (low values of a and c);

(ii) the proportion of significant conditioning factors obtained with landslide bodies as the grouping variable are generally lower than with the source areas grouping (Fig 6).

These findings can be explained by the fact that, on the one hand, large SUs encompass a large variability of conditioning factors causing the model not to be able to discriminate between stable and unstable SUs. On the other hand, smaller SUs contain a reduced number of conditioning factors allowing for an easier classification of the terrain conditions.

Table 3 presents the list and the number of times each conditioning factor is significant for each DEM spatial resolution and grouping variable. Taking the landslide source areas as the grouping variable, the mean and the standard deviation of the slope gradients and the slope curvatures are significant variables for all the DEMs and for more than 35% of the 56 model runs. The slope mean curvature is negatively

correlated with the landslide inventory indicating a tendency of absence of landslide source areas where transversal local convex profiles are present. Among the lithotypes, the weathered marls and the moraine are the most significant predictors. Further, the number of times each variable is significant is constant across the different DEMs.

Taking instead the landslide bodies as grouping variable, the results are different. The total number of times the predictors are significant is not constant with DEM resolution (20, 38 and 87 for the 5, 10 and 25 m spatial resolution DEMs, respectively). In particular, when the 5 m resolution DEM is used, only the standard deviation of the slope gradient appears as a significant predictor. The numbers of significant predictors increase slightly when we move to the 10 m spatial resolution DEM, for which the lithotypes are also significant predictors. Variables describing the terrain curvature are often significant, and are the only type of significant variable, when using the 25 m spatial resolution DEM.

Examination of the statistical significance of variables suggests that the results obtained using DEMs with 5 and 10-m resolutions and the presence/absence of landslides bodies as dependent variable are less robust than results obtained using the landslide source areas. Susceptibility maps prepared with the 10-m DEM exhibit a larger number of significant variables (99) and also a greater number of variables (5) which are significant more than 15 times out of 56. It is interesting to observe that land-use variables are never significant in any of the 56 LRM runs.

Based on this analysis, we deduced that the 10-m spatial resolution DEM with the landslide source areas as the dependent variable provide the optimal data combination for the preparation of the SU-based susceptibility zonation. We thus trained the LRM on a random selection of 70% of the SUs, reserving the remaining 30% for validation. Fig. 7a presents the landslide susceptibility map, in five

classes, and Fig. 7b shows a histogram with the percentages of the five probability classes subdivided as true positives and false positives. Fig. 8 shows the ROC plots of the susceptibility zonation for the training and the validation sets. The training set has an *AUC* value of 0.80 while the validation set has a value of 0.75; which we consider as satisfactory. Almost 12% of the study area is classified as of "very high" susceptibility with 8.5% of the study area corresponding to regions where landslide source areas are actually observed (true positives). About 37% of the study area is classified with a "high" susceptibility with 25% true positive. The histogram also indicates that a large extent of the area is classified as susceptible where no active landslides are observed.

7. Conclusions

We have proposed a procedure to determine the best DEM spatial resolution and the most appropriate way to use landslide information (landslide bodies vs. source areas) for landslide susceptibility zonation at a scale of 1:10,000. The procedure was developed within the framework of optimized slope units. Homogeneous SUs were produced automatically with the *r.slopeunits* software and optimal SU delineation parameters were determined following the procedure of Alvioli et al. (2016). We used three DEMs with spatial resolutions of 5, 10 and 25 m, and trained a logistic regression model with a large number of different sets of SUs using the presence/absence of landslide bodies or only the landslide source areas as dependent variables. We measured the performance of the logistic regression model as a function of the different SU delineations, with a metric function which makes use of a proper combination of an aspect segmentation metric and the standard *AUC* metric. Maximization of the objective function provides the best combination of input parameters for the terrain partitioning. We performed the maximization procedure six times, combining three different DEM resolutions with the choice of either landslide bodies or source areas. We compared the resulting six landslide susceptibility

maps on the basis of an analysis of the statistical significance of thematic and morphometric variables within the whole (*a*, *c*) region considered. This allowed us to identify a susceptibility map providing the most informative content. The map obtained with the 10-m DEM resolution and the landslide source areas was the most statistically reliable, and thus the optimal one. The final susceptibility map obtained using the aforementioned information was used to perform a spatial validation of the LRM, characterized by an *AUC* value of 0.75 and true positives percentages of 8.5% in the highest susceptibility class and 25% in the second highest class.

We have described a procedure which maximizes the reliability of the susceptibility map by extracting as much information as possible from the available conditioning factors, landslide information and DEM resolution, in conjunction with the use of proper mapping units such as SUs. We have further stressed the importance of carefully analyzing the statistical significance of the model used for the susceptibility zonation. Synthetic performance indices may report a relatively high performance, while the statistical significance of the results may simultaneously be poor, and this is often overlooked in the existing literature.

Acknowledgements

We thank the anonymous reviewers for their critical reviews of this paper. Mark Bebbington and Jean Van Campenhout carefully read and improved the manuscript. This work has been supported by the Marie Curie Research and Initial Training Network "CHANGES: Changing Hydro-meteorological Risks as Analyzed by a New Generation of European Scientists", funded by the European Community's 7th Framework Programme FP7/2007–2013 under Grant Agreement No. 263953. M. Alvioli was supported by a grant of the Department for Civil Protection.

M. Alvioli also acknowledges the CINECA award under ISCRA initiative for making high-performance computing resources available. Some information of the landslide inventory was provided by the RTM-04 (Restauration des Terrains en Montagne) service of Département des Alpes-de-Haute-Provence.

8. References

Aleotti, P., Chowdhury, R.N., 1999. Landslide hazard assessment: summary review and new perspectives. Bulletin of Engineering Geology and the Environment 58(1), 21–44. http://dx.doi.org/10.1007/s100640050066

Alvioli, M., Marchesini, I., Reichenbach, P., Rossi, M., Fiorucci, F., Ardizzone, F., Guzzetti, F., 2016. Automatic delineation of geomorphological slope units with r.slopeunits v1.0 and their optimization for landslide susceptibility modeling. Geoscientific Model Development 9, 3675-3991. http://dx.doi.org/10.5194/gmd-9-3975-2016

Ayalew, L., Yamagishi, H., 2005. The application of GIS-based logistic regression for landslide susceptibility mapping in the Kakuda-Yahiko Mountains, Central Japan. Geomorphology 65(1-2), 15–31. http://dx.doi.org/10.1016/j.geomorph.2004.06.010

Baillargeon, S., 2005. Le krigeage: revue de la théorie et application à l'interpolation spatiale de données de précipitations. Mémoire de Maîtrise ès Sciences de la Faculté des Études Supérieures de l'Université de Laval. M.Sc. Thesis, Université Laval Quebec. http://www.theses.ulaval.ca/2005/22636/ (Last accessed: January 10th, 2017)

Bernknopf, R.L., Cambell, R.H., Brookshire, D.S., Shapiro, C.D., 1988. A probabilistic approach to landslide hazard mapping in Cincinnati, Ohio, with applications for economic evaluation. Bulletin of the International Association of Engineering Geology 25, 39–56. http://dx.doi.org/10.2113/gseegeosci.xxv.1.39

Brenning, A., 2005. Spatial prediction models for landslide hazards: review, comparison and evaluation. Natural Hazards and Earth System Science 5(6), 853–862. http://dx.doi.org/ 10.5194/nhess-5-853-2005

Carrara, A., 1988. Drainage and divide networks derived from high-fidelity digital terrain models. In C. F. Chung, A. G. Fabbri, & R. Sinding-Larsen, eds. Quantitative analysis of mineral and energy resources, NATO-ASI Series. Dordrecht, The Netherlands: D. Reidel Publishing Co., 581–597. http://dx.doi.org/10.1007/978-94-009-4029-1_34

Carrara, A., Cardinali, M., Detti, R., Guzzetti, F., Pasqui, V., Reichenbach, P., 1991. GIS techniques and statistical models in evaluating landslide hazard. Earth Surface Processes and Landforms 16, 427–445. http://dx.doi.org/10.1002/esp.3290160505

Carrara, A., Cardinali, M., Guzzetti, F., Reichenbach, P., 1995. GIS technology in mapping landslide hazard. In A. Carrara & F. Guzzetti, eds. Assessing Natural Hazards. Vol. 5 of Advances in Natural and Technological Hazards Research. Dordrecht: Kluwer Academic Publishers, 135–175. http://dx.doi.org/10.1007/978-94-015-8404-3_8

Catani, F., Lagomarsino, D., Segoni, S., Tofani, V., 2013. Landslide susceptibility estimation by random forests technique: sensitivity and scaling issues. Natural Hazards and Earth System Sciences 13(11), 2815–2831. http://dx.doi.org/10.5194/nhess-13-2815-2013

Claessens, L., Heuvelink, G.B.M., Schoorl, J.M., Veldkamp, A., 2005. DEM resolution effects on shallow landslide hazard and soil redistribution modelling. Earth Surface Processes and Landforms 30(4), 461–477. http://dx.doi.org/10.1002/esp.1155

Corominas, J., van Westen, C.J., Frattini, P., Cascini, L., Malet, J.-P., Fotopoulou, S., Catani, F., van den Eeckhaut, M., Mavrouli, O.-C., Agliardi, F., Pitilakis, K., Winter, M.G., Pastor, M., Ferlisi, S., Tofani, V., Hervás, J., Smith, J.T., 2014. Recommendations for the quantitative assessment of landslide risk. Bulletin of Engineering Geology and the Environment 73(2), 209-263. http://dx.doi.org/10.1007/s10064-013-0538-8

Cox, D.R., 1958. The regression analysis of binary sequences. Journal of the Royal Statistical

Society. Series B (Methodological) 20(2), 215–242. http://www.jstor.org/stable/2983890 (Last accessed: January 10th, 2017)

Dietrich, W.E, Bellugi, D., Real de Asua, R., 2001. Validation of shallow landslide model, SHALTAB, for forest management. In: M.S. Wigmosta, S.J. Burges (Eds.), Land use and watersheds: human influence on hydrology and geomorphology in urban and forest areas - Water Science and Application Series. American Geophysical Union, Washington, DC, USA, 2, 195-227. http://dx.doi.org/10.1029/WS002

van den Eeckhaut, M., Reichenbach, P., Guzzetti, F., Rossi, M., Poesen, J., 2009. Combined landslide inventory and susceptibility assessment based on different mapping units: an example from the Flemish Ardennes, Belgium. Natural Hazards and Earth System Sciences 9, 507–521. http://dx.doi.org/10.5194/nhess-9-507-2009

Ercanoglu, M., 2005. Landslide susceptibility assessment of SE Bartin (West Black Sea region, Turkey) by artificial neural networks. Natural Hazards and Earth System Sciences 5(6), 979–992. http://dx.doi.org/10.5194/nhess-5-979-2005

Espindola, G.M., Camara, G., Reis, I.A., Bins, L.S., Monteiro, A.M., 2006. Parameter selection for region-growing image segmentation algorithms using spatial autocorrelation. International Journal of Remote Sensing 27(14), 3035–3040. http://dx.doi.org/10.1080/01431160600617194

Fell, R., Corominas, J, Bonnard, C, Cascini, L, Leroi, E, Savage W. Z on behalf of the JTC-1 Joint Technical Committee on Landslides and Engineered Slopes, 2008. Guidelines for Landslide Susceptibility, Hazard and Risk Zoning for Land Use Planning. Engineering Geology 102(3-4), 99–111. http://dx.doi.org/10.1016/j.enggeo.2008.03.014

Flageollet, J.-C., Maquaire, O., Martin, B., Weber, D., 1999. Landslides and climatic conditions in

the Barcelonnette and Vars basins (Southern French Alps, France). Geomorphology 30, 65–78. http://dx.doi.org/10.1016/S0169-555X(99)00045-8

Frattini P., Crosta G., Carrara A., 2010. Techniques for evaluating the performance of landslide susceptibility models. Engineering Geology 111, 62–72. http://dx.doi.org/10.1016/j.enggeo.2009.12.004

Fuchs, M., Torizin, J., Kühn, F., 2014. The effect of DEM resolution on the computation of the factor of safety using an infinite slope model. Geomorphology 224, 16–26. http://dx.doi.org/10.1016/j.geomorph.2014.07.015

GRASS Development Team, 2016. Geographic Resources Analysis Support System (GRASS) Software, Version 7.0. Open Source Geospatial Foundation. http://grass.osgeo.org (Last accessed: January 10th, 2017)

Guzzetti, F., 2006. Landslide hazard and risk assessment. PhD Thesis, University of Bonn, Bonn, Germany. http://hss.ulb.uni-bonn.de/2006/0817/0817.pdf (Last accessed: January 10th, 2017)

Guzzetti, F., Reichenbach, P., Ardizzone, F., Cardinali, M., Galli, M., 2006. Estimating the quality of landslide susceptibility models. Geomorphology 81, 166–184. http://dx.doi.org/10.1016/j.geomorph.2006.04.007

Guzzetti, F., Carrara, A., Cardinali, M., Reichenbach, P., 1999. Landslide hazard evaluation: a review of current techniques and their application in a multi-scale study, Central Italy. Geomorphology 31, 181–216. http://dx.doi.org/10.1016/S0169-555X(99)00078-1

Hanley, J.A., McNeil, B.J., 1982. The Meaning and Use of the Area under a Receiver Operating Characteristic (ROC) Curve. Radiology 143, 29–36. https://dx.doi.org/10.1148/radiology.143.1.7063747

InterMap, 2008. Product Handbook & Quick Start Guide, InterMap. http://www.intermap.com (Last accessed: January 10th, 2017)

Kanungo D., Arrora M., Sarkar S., Gupta R., 2009. Landslide Susceptibility Zonation (LSZ) mapping-a review. Journal of South Asia Disaster Studies 2, 81–105.

Krige, D.G., 1966. Two dimensional weighted moving average trend surfaces for ore-evaluation. Journal of the South African Institute of Mining and Metallurgy 66, 13–38. http://saimm.org.za/Conferences/DanieKrige/DGK10.pdf (Last accessed: January 10th, 2017)

Legorreta Paulín, G, Bursik, M., Lugo-Hubp, J., Zamorano Orozco, J.J., 2010. Effect of Pixel Size on Cartographic Representation of Shallow and Deep-Seated Landslide, and Its Collateral Effects on the Forecasting of Landslides by SINMAP and Multiple Logistic Regression Landslide Models. Physics and Chemistry of the Earth 35(3-5), 137–48 http://dx.doi.org/10.1016/j.pce.2010.04.008

Legorreta Paulín, G, Pouget, S., Bursik, M., Aceves Quesada, F., Contreras, T., 2016. Comparing Landslide Susceptibility Models in the Río El Estado Watershed on the SW Flank of Pico de Orizaba Volcano, Mexico. Natural Hazards 80(1), 127–39. http://dx.doi.org/10.1007/s11069-015-1960-y

Maire, C., Datcu, M., Audenino, P., 2003. SAR DEM filtering by mean of Bayesian and multi-scale non-stationary methods. International Geoscience and Remote Sensing Symposium (IGARSS), 21-25 July, Toulouse, France, 3916–3918. https://doi.org/10.1109/IGARSS.2003.1295313

Malet, J.-P., Thiery, Y., Maquaire, O., Puissant, A., 2006. Landslide susceptibility, vulnerability and risk assessment through GIS procedures: a tentative application in the South French Alps. Revue Internationale de Géomatique, European Journal of GIS and Spatial Analysis 16(3-4), 499-

525.

Maquaire, O., Malet, J.-P., Remaître, A., Locat, J., Klotz, S., Guillon, J., 2003. Instability conditions of marly hillslopes: towards landsliding or gullying? The case of the Barcelonnette Basin, South East France. Engineering Geology 70(1-2), 109–130. http://dx.doi.org/10.1016/S0013-7952(03)00086-3

Moravek, A., 2011. Modelling landcover changes in the Barcelonnette Basin at very high resolution. MSc Thesis, Department of Geography, University of Strasbourg, 45p.

Ohlmacher, G.C., Davis, J.C., 2003. Using multiple logistic regression and GIS technology to predict landslide hazard in northeast Kansas, USA. Engineering Geology 69(3-4), 331–343.

Pardeshi S.D., Autade S.E., Pardeshi S.S., 2013. Landslide hazard assessment: recent trends and techniques. SpringerPlus, 2, 523. http://dx.doi.org/10.1016/S0013-7952(03)00069-3

Remaître, A., Malet, J., Maquaire, O., 2005. Morphology and sedimentology of a complex debris flow in a clay-shale basin. Earth Surface Processes and Landforms 30, 339–348. http://dx.doi.org/10.1002/esp.1161

Remaître, A., Malet, J.-P., 2010. The effectiveness of torrent check dams to control channel instability: example of debris-flow events in clay shales. In C. C. Garcia & M. A. Lenzi, eds. Check Dams, Morphological Adjustments and Erosion Control in Torrential Streams. Nova Science Publishers, 211–237. ISBN: 978-1-60876-146-3

Rossi, M., Guzzetti, F., Reichenbach, P., Mondini, A.C., Peruccacci, S., 2010. Optimal landslide susceptibility zonation based on multiple forecasts. Geomorphology 114(3), 129–142.

http://dx.doi.org/10.1016/j.geomorph.2009.06.020

Rossi, M. and Reichenbach, P., 2016. LAND-SE: a software for statistically based landslide

susceptibility zonation, version 1.0, Geosci. Model Dev., 9, 3533-3543. http://dx.doi.org/10.5194/gmd-9-3533-2016

Schlögel, R., Malet, J.-P., Remaître, A., Reichenbach, P., Doubre, C., 2015. Analysis of a landslide multi-date inventory in a complex mountain landscape: the Ubaye valley case study. Natural Hazards and Earth System Sciences 15, 2369–2389. http://dx.doi.org/10.5194/nhess-15-2369-2015

Stevenson, J.A., Sun, X., Mitchell, N.C., 2010. Despeckling SRTM and other topographic data with a denoising algorithm. Geomorphology 114(3), 238–252. http://dx.doi.org/10.1016/j.geomorph.2009.07.006

Thiery, Y., 2007. Susceptibilité du Bassin de Barcelonnette (Alpes du Sud, France) aux "mouvements de versant" : cartographie morpho-dynamique, analyse spatiale et modélisation probabiliste. Thèse de Doctorat, Université de Caen Basse-Normandie. https://tel.archives-ouvertes.fr/tel-00259135 (Last accesed: January 10th, 2017)

Thiery, Y., Malet, J.-P., Sterlacchini, S., Puissant, A., Maquaire, O., 2007. Landslide susceptibility assessment by bivariate methods at large scales: application to a complex mountainous environment. Geomorphology 92(1), 38–59. http://dx.doi.org/10.1016/j.geomorph.2007.02.020

Tian, Y., Xiao, C., Liu, Y., Wu, L., 2008. Effects of raster resolution on landslide susceptibility mapping: A case study of Shenzhen. Science in China, Series E: Technological Sciences 51(2007), 188–198. http://dx.doi.org/10.1007/s11431-008-6009-y

Wieczorek, G.F., Gori, P.L., Jager, S., Kappel, W.M., Negussy, D., 1996. Assessment and management of landslide hazards near Tully Valley landslide, Syracuse, New York, USA. In Proc VII Int. Symp. Landslides, Trondheim, June 1966, 1. Balkema, Rotterdam, 411–416.

Table 1. Combination of parameters *c* and *a* maximizing *S*(*a*,*c*) for each DEM and landslide representation (body, source area).

	Landslide body		**Landslide source area**	
	a (m^2)	*c*	*a* (m^2)	*c*
DEM 5 m	64.000	0.089	74.800	0.098
DEM 10 m	53.200	0.142	53.200	0.142
DEM 25 m	409.600	0.045	398.800	0.045

Table 2. Mean and standard deviations of the SU sizes obtained with the optimal combination of parameters in Table 1.

	Landslide body		**Landslide source area**	
	SU mean size (m^2)	Std. dev. of SU size (m^2)	SU mean size (m^2)	Std. dev. of SU size (m^2)
DEM 5 m	153.252	180.283	184.420	219.984
DEM 10 m	223.966	348.358	223.966	348.358
DEM 25 m	475.806	277.175	470.164	275.562

Table 3. Significance of the conditioning factors for the three DEMs computed for the 56 LRMs with the SUs presented in Fig. 2. The significance of the predictors is indicated for, respectively, the use of landslide body or source area as the dependent variable.

	Landslide body		**Landslide source area**	
	#	Conditioning factor	#	Conditioning factor
DEM 5 m	13	Standard deviation of slope gradient	21	Standard deviation of slope gradient
	2	Mean slope gradient	16	Mean slope gradient
	3	Marly-Limestone	11	Mean slope profile curvature
	1	Mean slope planar curvature	7	Mean slope planar curvature
	1	Mean slope profile curvature	5	Moraine
			5	Weathered marls
			3	Marly-Limestone
			2	Standard deviation of slope profile curvature
			1	Standard deviation of slope planar curvature

	11	Weathered marls	19	Weathered marls
	8	Moraine	18	Mean slope gradient
	6	Marly-Limestone	17	Mean slope profile curvature
	3	Standard deviation of slope profile curvature	17	Moraine
DEM	2	Limestone	16	Std Slope
10 m	2	Scree of blocks	5	Scree of blocks
	2	Mean slope profile curvature	4	Standard deviation of slope profile curvature
	2	Standard deviation of slope planar curvature	2	Marly-Limestone
	1	Standard slope gradient	1	Mean slope planar curvature
	1	Sandstone/gypsum		
	32	Standard deviation of slope profile curvature	29	Mean slope planar curvature
	30	Mean slope planar Curvature	20	Mean slope gradient
	9	Marly-Limestone	9	Weathered marls
	5	Weathered marls	7	Standard deviation of slope profile curvature
DEM	3	Moraine	6	Moraine
25 m	3	Mean slope	4	Standard deviation of slope gradient
	2	Limestone	3	Marly-Limestone
	1	Scree of blocks	2	Scree of blocks
	1	Standard deviation of slope gradient		
	1	Mean slope profile curvature		

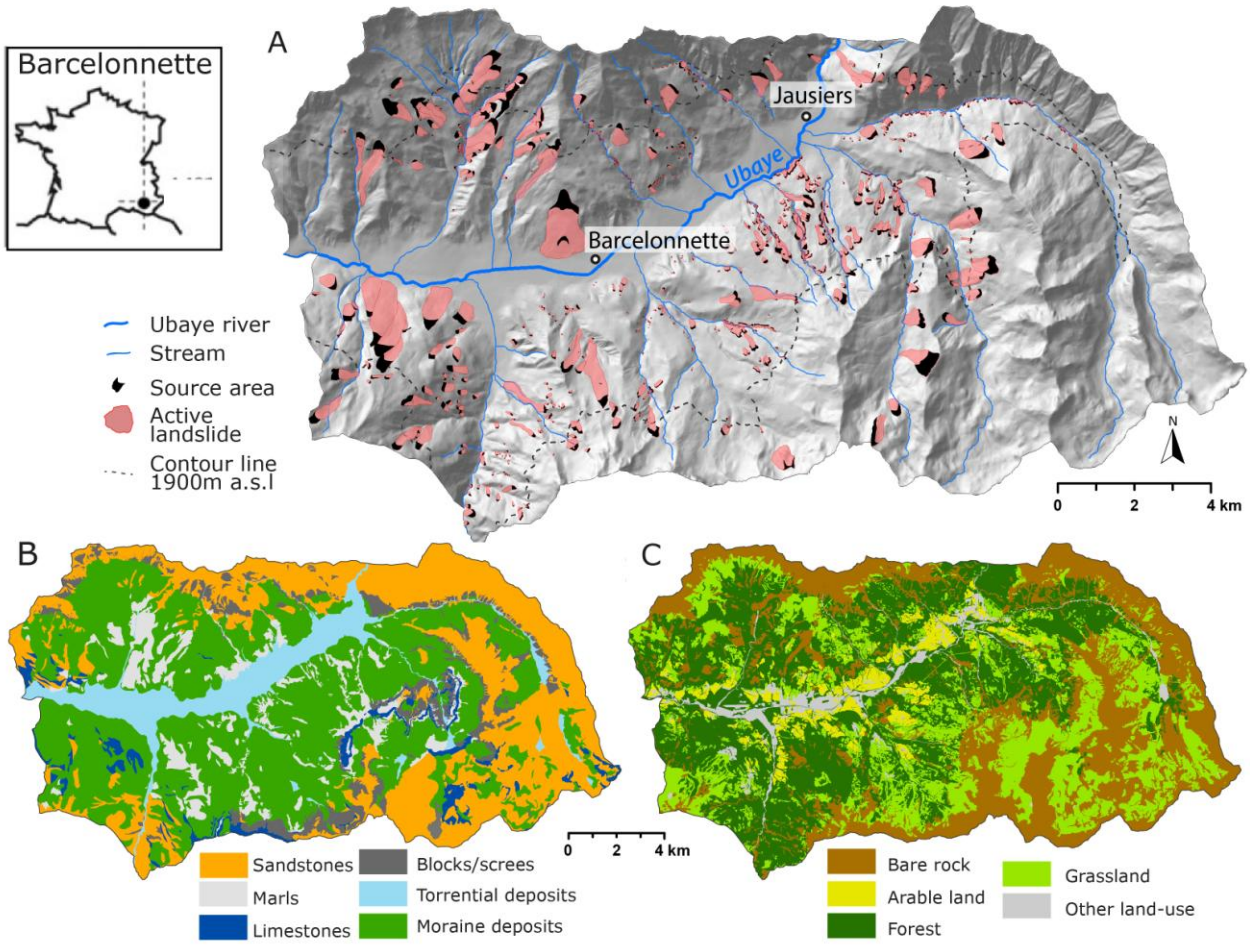

Fig. 1. Environmental settings of the Ubaye valley (South East France) and an associated landslide inventory map. (A) Active landslides represented on a shaded relief created on a 10 m spatial resolution DEM. (B) Simplified lithological map issued from the BRGM geological maps at 1:50.000. (C) Land cover map modified after Moravek, (2011) based on the photo-interpretation of the 2004 airborne orthophotographs.

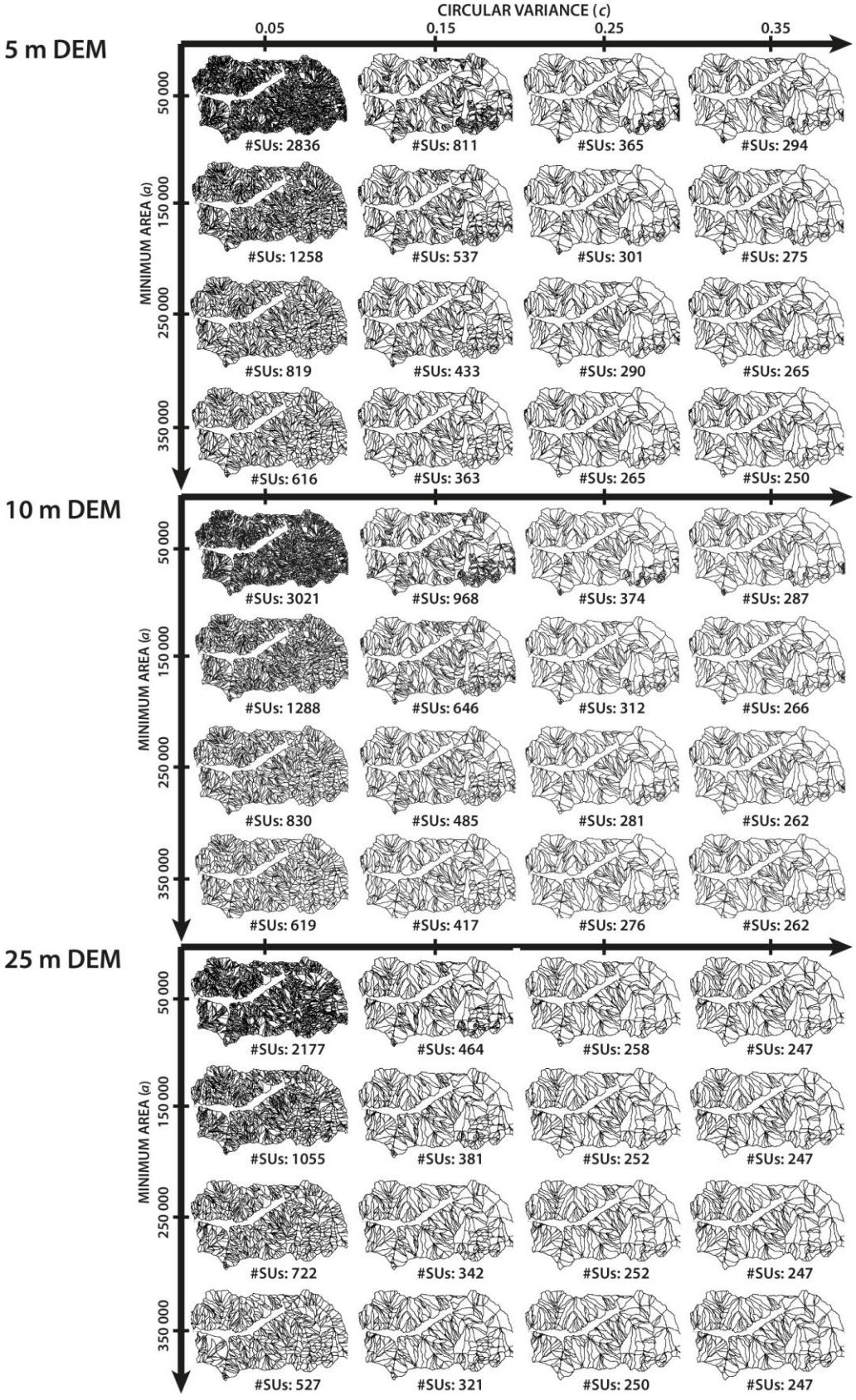

Fig. 2. SU delineation obtained with *r.slopeunits* for several combinations of *a* and *c* input parameters. The figure shows the

number of SUs (i.e. #SUs) obtained with the 5-m, 10-m and 25-m resolution DEM (top, center and bottom, respectively).

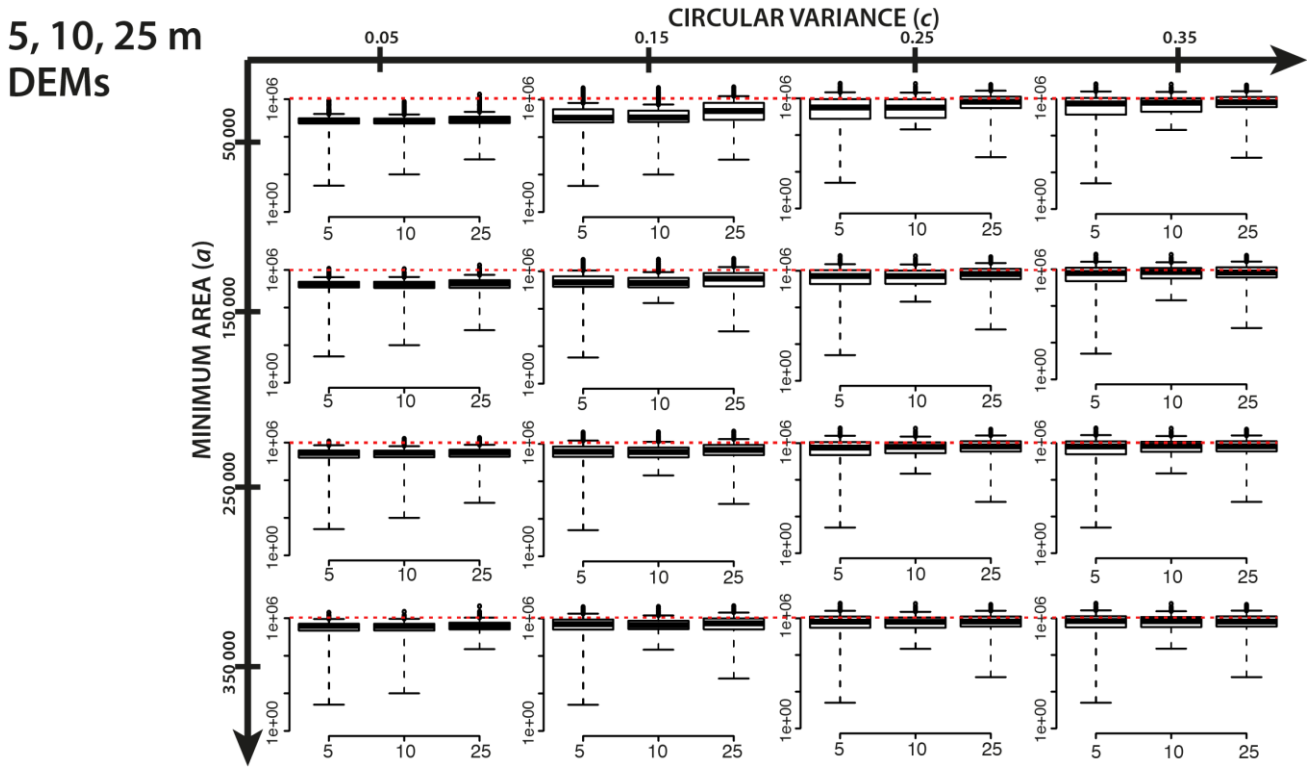

Fig. 3. Boxplot statistics of the SU sizes obtained from the 5, 10 and 25 m resolution DEMs, respectively, for the same combinations of the (*a*, *c*) parameters shown in Fig. 2. Red dotted lines show the area corresponding to 1×10^6 m^2.

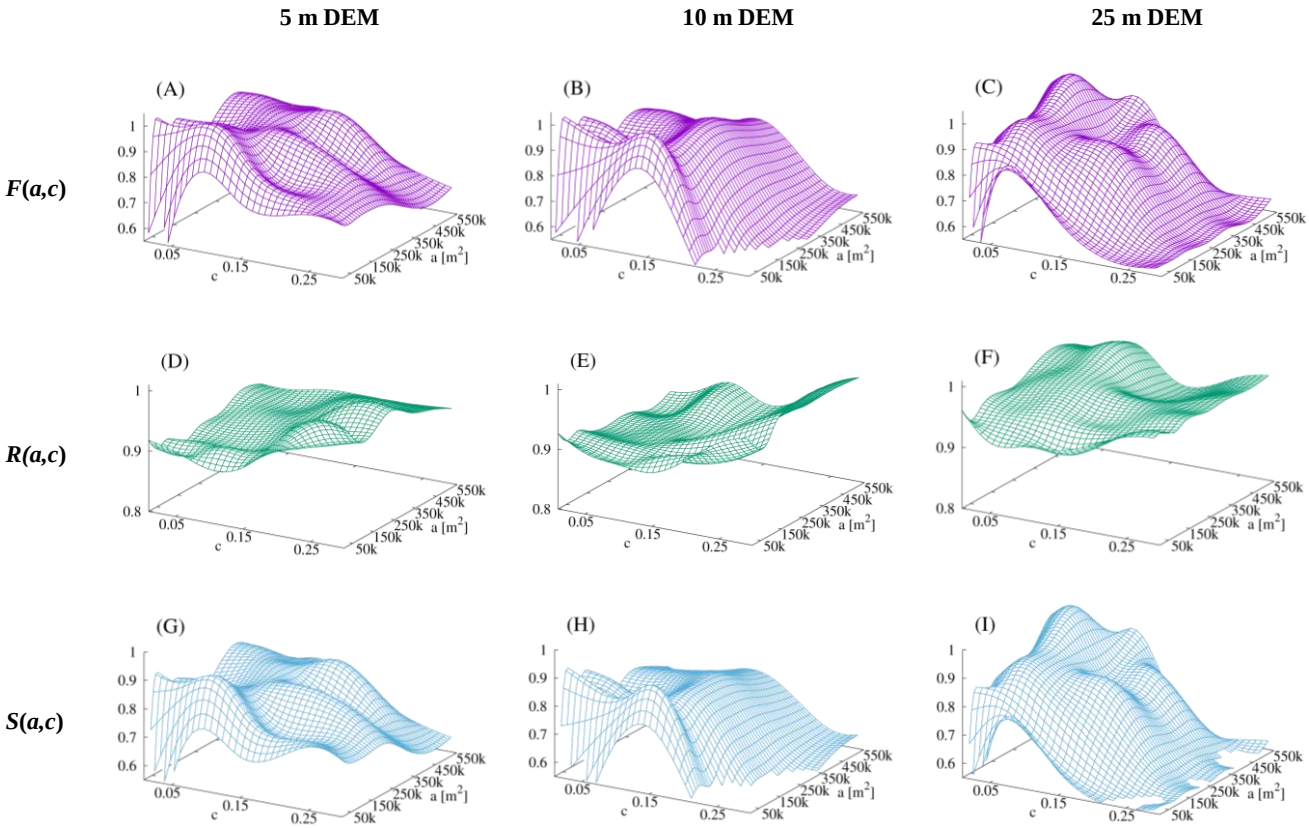

Fig. 4. Statistical indicators of the logistic regression model: aspect segmentation metric $F(a, c)$ (A)-(C), *AUC* metric $R(a, c)$ (D)-(F) and the product of the two quantities $S(a, c)$ (G)-(I), normalized to their maxima, as in Eq. (4) evaluated for the three DEMs. The *AUC* metric corresponds to the LRM evaluated considering the landslide bodies as the grouping variable. In the figures, the values are interpolated using a finer grid with respect to the 56 combinations.

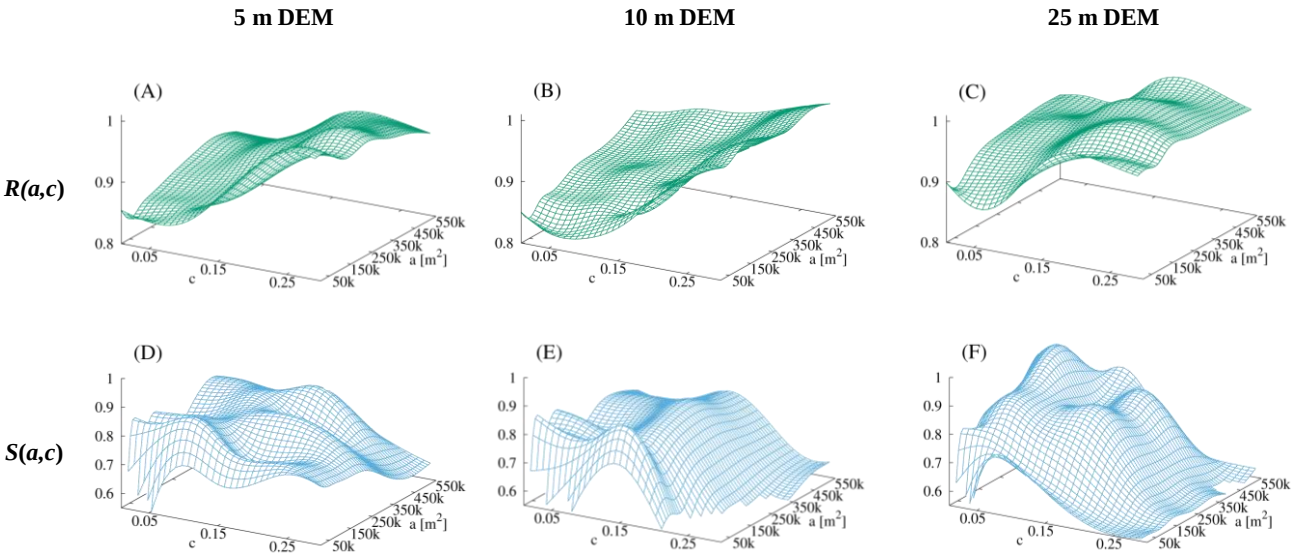

Fig. 5. Statistical indicators of the Logistic Regression Models: *AUC* metric *R*(*a*, *c*) (A)-(C) and the product of the two quantities S(*a*, *c*) (D)-(F), normalized to their maxima as in Eq. (4), evaluated for the three DEMs. The *AUC* corresponds to the LRM evaluated with the landslide source areas as the grouping variable. In the figures, the values are interpolated using a finer grid with respect to the 56 combinations.

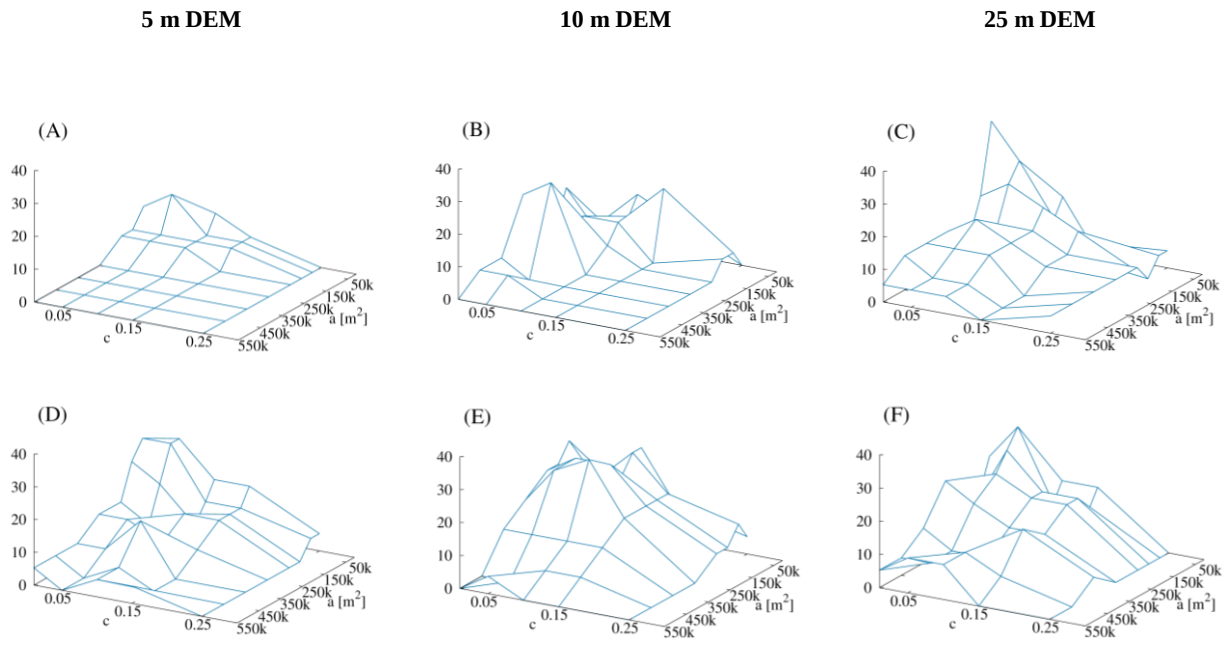

Fig. 6. Percentages of relevant variables in the Logistic Regression Model as a function of the (*a*, *c*) input parameters. The graphs show results obtained considering the landslide bodies (A)-(C) and the source areas (D)-(F). Note that the direction of the *a* axis differs from the direction of the same axis in Fig. 4 and 5.

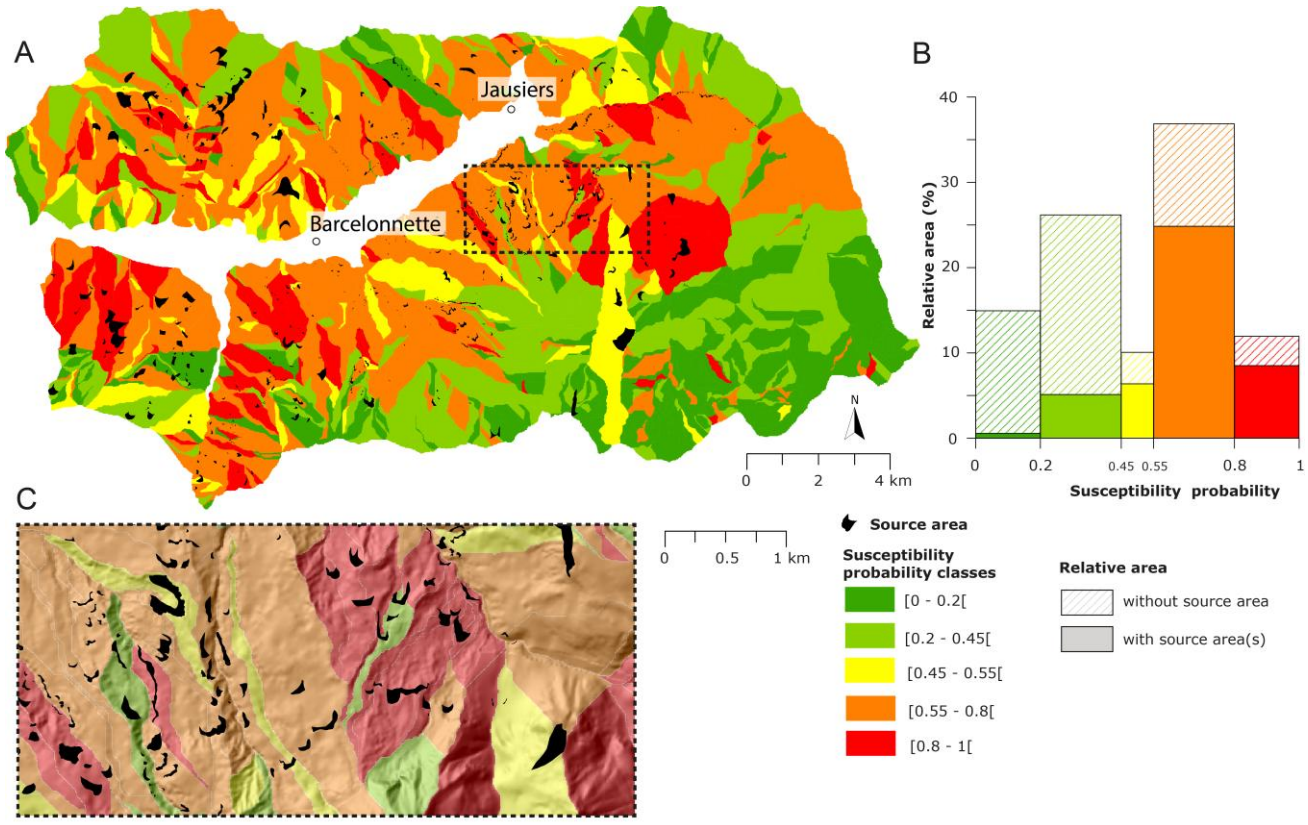

Fig. 7. Landslide susceptibility zonation analysis. (A) Optimal landslide susceptibility map classified in five classes. (B) Histogram presenting the distribution of the probability classes. (C) Zoom on the 'Bois Noir' sub-region to illustrate the spatial resolution of the model.

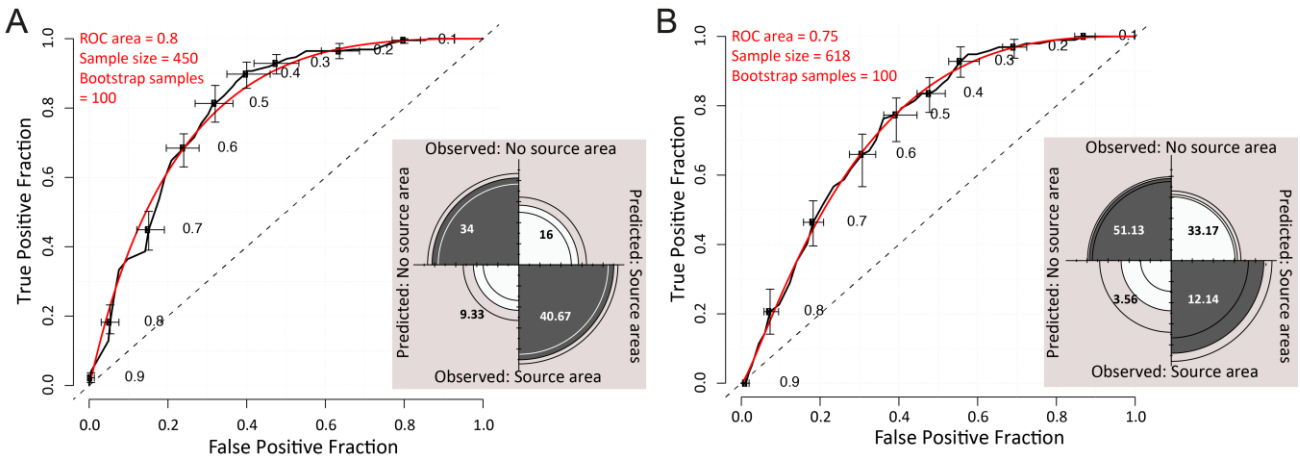

Figure 8. ROC curve evaluation and four fold plots of the training (A) and validation (B) model using the source areas as the dependent variable at 10 m DEM resolution.